

Research paper

A practical and efficient numerical method for the Cahn–Hilliard equation in complex domains

Darae Jeong^a, Junxiang Yang^b, Junseok Kim^{b,*}

^a Department of Mathematics, Kangwon National University, Gangwon-do 24341, Republic of Korea

^b Department of Mathematics, Korea University, Seoul 02841, Republic of Korea



ARTICLE INFO

Article history:

Received 4 May 2018

Revised 11 January 2019

Accepted 12 February 2019

Available online 13 February 2019

Keywords:

Ternary Cahn–Hilliard system

Cahn–Hilliard equation

Complex domain

Phase separation

Multigrid method

ABSTRACT

In this article, we present a practical and efficient numerical method for the Cahn–Hilliard (CH) equation in the two- and three-dimensional complex domains. We propose a simple mathematical model for the binary mixture in the complex domains. The model is based on the ternary CH system. An arbitrary domain is represented by the third phase, which is fixed during the temporal evolution of the other phases. By the local conservative property of the sum of the phases, the governing equation is simplified to a binary CH equation with a source term. For the numerical solution, we use a practically unconditionally gradient stable scheme. Various numerical experiments are performed on arbitrary domains. The numerical results show that the proposed algorithm can deal with the complex domains efficiently.

© 2019 Elsevier B.V. All rights reserved.

1. Introduction

A phase-field model is a mathematical model for describing and solving interfacial problems such as solidification, motion by mean curvature, image segmentation, microstructure evolution, viscous fingering, fracture, multiphase fluid flow, and vesicle dynamics [1]. In the phase-field model, boundary conditions at the interface is replaced by a partial differential equation for the evolution of an order parameter, which is also called by the phase-field. This phase-field has two different values (for example, 0 and 1) in each of the phases and there is a smooth and finite transition layer between both values along the interface. The position of the interface can be defined as a level set of the phase-field function. A phase-field model is typically constructed to recover the correct interfacial dynamics as the interface width approaches zero. With this phase-field model, we can deal with the interfacial problems by solving partial differential equations for the whole domain and avoid the explicit treatment of the boundary conditions at the interface. Typically, the Cahn–Hilliard (CH) [2] and the Allen–Cahn (AC) [3] equations are used for the conserved and non-conservative phase-fields, respectively. As a similar approach, there is density-gradient theory for interfacial problems. Kou and Sun [4] proposed thermodynamically consistent modeling and presented simulation of multi-component two-phase fluid flow with partial miscibility

In this study, we consider a new simple numerical method for the CH equation in complex domains. The CH equation is a mathematical model to describe phase separation in a binary alloy and has been applied to many areas of scientific fields [5–10]. See [11] for the physical, mathematical, and numerical derivations of the CH equation. See [12] for a benchmark

* Corresponding author.

E-mail address: cfdkim@korea.ac.kr (J. Kim).

URL: <http://math.korea.ac.kr/~cfdkim/> (J. Kim)

problem for the CH equation. Areias et al. [13] developed an efficient staggered algorithm for the CH equation and finite strain elasticity. They also presented isogeometric analysis with strong multipatch C^1 -coupling for the CH equation in [14]. The numerical methods for the CH equation in irregular domains have been developed [15–17]. Shin et al. [15] proposed a numerical method for the CH equation in non-regular domains by imposing a boundary control function. Li et al. [16] developed a conservative numerical method for the CH equation with Dirichlet boundary conditions in arbitrary domains. Aland et al. [17] combined a diffuse-domain method with a phase-field method for studying the two-phase flow in complex geometries, the complex internal boundary conditions are imposed on implicit solid domain by using source terms.

Unlike the previous numerical methods, our proposed method is very simple to treat the CH equation in complex domains. In this study, the proposed mathematical model for the binary mixture is based on the ternary CH system which models the phase separation of a three-component mixture. Here, a complex domain is defined by a level-set of the third phase, which is fixed during the temporal evolution of the other two phases. By the locally conservative property of the sum of the three phases, we only need to solve a binary CH equation with a source term.

Furthermore, after a small modification (i.e., adding the source term) of the pre-existing codes (e.g., Fourier spectral method [18–20], finite element method [21–24], and isogeometric method [25–27]) for the CH equation, the proposed algorithm can be straightforwardly implemented.

The contents of this paper are organized as follows. In Section 2, we describe the proposed governing equation for phase separation in the arbitrary domains. In Section 3, we present a nonlinear splitting finite difference scheme for the modified CH equation. We present computational experiments in Section 4. Finally, conclusions are drawn in Section 5.

2. Modified Cahn–Hilliard equation

To derive the modified CH equation in the complex domain, we first consider the evolution of the ternary CH system in a domain $\Omega \subset \mathbb{R}^d$, where $d = 2$ and 3 are space dimensions. Let $c_i(\mathbf{x}, t)$ for $i = 1, 2, 3$ be the mole fraction of each component in the ternary mixture as a function of space \mathbf{x} and time t . By the mass conservation, the total sum of mole fractions must be to 1, i.e.,

$$c_1(\mathbf{x}, t) + c_2(\mathbf{x}, t) + c_3(\mathbf{x}, t) = 1. \tag{1}$$

We consider the Helmholtz free energy functional from the generalized Ginzburg–Landau form [28] as follows:

$$\mathcal{F}(c_1, c_2, c_3) = \int_{\Omega} \sum_{i=1}^3 \left(F(c_i) + \frac{\epsilon^2}{2} |\nabla c_i|^2 \right) d\mathbf{x}, \tag{2}$$

where $F(c_i) = 0.25c_i^2(c_i - 1)^2$ and $\epsilon > 0$ is the gradient energy coefficient. The temporal evolution equation of c_i is given by the following ternary CH system:

$$\frac{\partial c_i}{\partial t} = \Delta \mu_i, \tag{3}$$

$$\mu_i = f(c_i) - \epsilon^2 \Delta c_i + \beta(c_1, c_2, c_3), \quad \text{for } i = 1, 2, 3, \tag{4}$$

where $f(c_i) = F'(c_i) = c_i(c_i - 0.5)(c_i - 1)$ and $\beta(c_1, c_2, c_3) = -\frac{1}{3} \sum_{i=1}^3 f(c_i) = -c_1 c_2 c_3$. More details about the Lagrangian multiplier $\beta(c_1, c_2, c_3)$ can be found in [29,30] and references therein. At boundary, the homogeneous Neumann conditions are used as follows:

$$\mathbf{n} \cdot \nabla c_i = 0 \text{ and } \mathbf{n} \cdot \nabla \mu_i = 0 \quad \text{on } \partial\Omega, \tag{5}$$

where \mathbf{n} is the unit normal vector to $\partial\Omega$.

In the proposed method, we utilize c_3 to represent an arbitrary domain, $\tilde{\Omega} \subset \Omega$. That is, $c_3 \approx 0$ on $\tilde{\Omega}$ and $c_3 \approx 1$ on $\Omega \setminus \tilde{\Omega}$. As shown in Fig. 1, we consider the 0.5-level set of c_3 as the domain boundary, $\partial\tilde{\Omega}$.

In fact, we only need to solve the equation for the phase c_1 because c_3 is fixed and c_2 can be defined as $c_2 = 1 - c_1 - c_3$ by the condition (1). Therefore, the proposed modified CH equation is simplified as

$$\frac{\partial c_1}{\partial t} = \Delta \mu_1, \tag{6}$$

$$\mu_1 = f(c_1) - \epsilon^2 \Delta c_1 - c_1(1 - c_1 - c_3)c_3, \tag{7}$$

which is the classical binary CH equation with a nonlinear source term.

3. Numerical solution

The governing equation is the classical binary CH equation with a nonlinear source term. Therefore, we can use many available numerical methods such as finite element method [21–24,31,32], finite difference method [15–17], Fourier spectral method [18–20], isogeometric method [25–27], multigrid method [33,34], and smoothed particle hydrodynamics (SPH) method [35]. In this paper, we use the finite difference scheme with a nonlinear multigrid method.

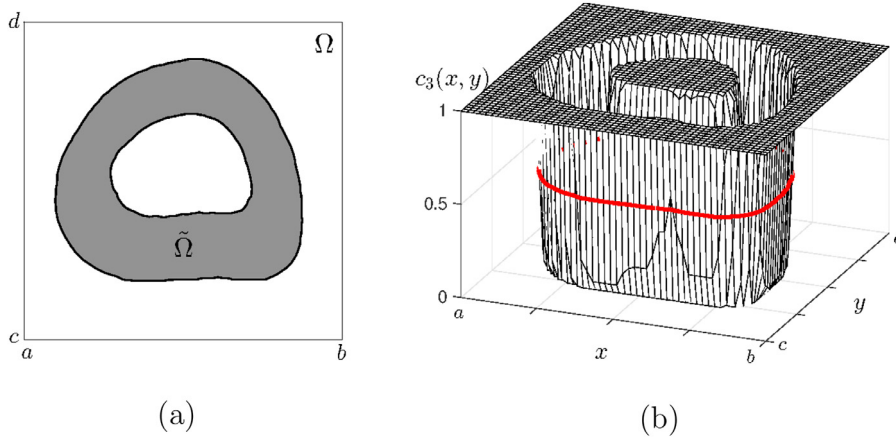


Fig. 1. Schematic illustrations of (a) the computational domain Ω and the arbitrary domain $\tilde{\Omega}$; (b) $c_3(x, y)$ in the two-dimensional space $\Omega = (a, b) \times (c, d)$.

Let $\Omega = (a, b) \times (c, d)$ be the two-dimensional computational domain. Let N_x and N_y be positive even integers, $h = (b - a)/N_x = (d - c)/N_y$ be the uniform mesh size, Δt be the time step size, and $\Omega_h = \{(x_i, y_j) : x_i = a + (i - 0.5)h, y_j = c + (j - 0.5)h, 1 \leq i \leq N_x, 1 \leq j \leq N_y\}$ be the set of cell-centers. Let c_{ij}^n and μ_{ij}^n be approximations of $c(x_i, y_j, n\Delta t)$ and $\mu(x_i, y_j, n\Delta t)$ with the time level n . Then, Eqs. (6) and (7) are discretized by using a nonlinear convex splitting type scheme [36,37]:

$$\frac{c_{1,ij}^{n+1} - c_{1,ij}^n}{\Delta t} = \Delta_h \mu_{1,ij}^{n+1}, \tag{8}$$

$$\begin{aligned} \mu_{1,ij}^{n+1} = & f(c_{1,ij}^{n+1}) + \frac{1}{4}c_{1,ij}^{n+1} - \frac{1}{4}c_{1,ij}^n - \epsilon^2 \Delta_h c_{1,ij}^{n+1} \\ & - c_{1,ij}^n (1 - c_{1,ij}^n - c_{3,ij}^n) c_{3,ij}^n, \end{aligned} \tag{9}$$

where the discrete Laplacian is given as $\Delta_h \phi_{ij} = (\phi_{i+1,j} + \phi_{i-1,j} + \phi_{i,j+1} + \phi_{i,j-1} - 4\phi_{ij})/h^2$ for $i = 1, \dots, N_x$ and $j = 1, \dots, N_y$. We solve Eqs. (8) and (9) as a coupled system of $c_{1,ij}^{n+1}$ and $\mu_{1,ij}^{n+1}$. At the computational domain boundary $\partial\Omega_h$, we use the zero Neumann boundary condition (5) as follows:

$$\begin{aligned} c_{1,0,j} &= c_{1,1,j}, \quad c_{1,N_x+1,j} = c_{1,N_x,j}, \quad c_{1,i,0} = c_{1,i,1}, \quad c_{1,i,N_y+1} = c_{1,i,N_y}, \\ \mu_{1,0,j} &= \mu_{1,1,j}, \quad \mu_{1,N_x+1,j} = \mu_{1,N_x,j}, \quad \mu_{1,i,0} = \mu_{1,i,1}, \quad \mu_{1,i,N_y+1} = \mu_{1,i,N_y}. \end{aligned}$$

The above discrete systems are solved by a full approximation storage (FAS) multigrid method with a Gauss–Seidel relaxation [38]. For more details about the multigrid method for the CH equation, we refer the reader to [39].

Similarly to the two-dimensional space, we define the computational domain $\Omega = (a, b) \times (c, d) \times (e, f)$ in the three-dimensional space. Let N_x, N_y , and N_z be positive even integers, $h = (b - a)/N_x = (d - c)/N_y = (f - e)/N_z$ be the uniform mesh size, and $\Omega_h = \{(x_i, y_j, z_k) : x_i = a + (i - 0.5)h, y_j = c + (j - 0.5)h, z_k = e + (k - 0.5)h, 1 \leq i \leq N_x, 1 \leq j \leq N_y, 1 \leq k \leq N_z\}$ be the set of cell-centers. Let c_{ijk}^n and μ_{ijk}^n be approximations of $c(x_i, y_j, z_k, n\Delta t)$ and $\mu(x_i, y_j, z_k, n\Delta t)$. Eqs. (6) and (7) are also discretized by using a nonlinear convex splitting type scheme as

$$\frac{c_{1,ijk}^{n+1} - c_{1,ijk}^n}{\Delta t} = \Delta_h \mu_{1,ijk}^{n+1}, \tag{10}$$

$$\begin{aligned} \mu_{1,ijk}^{n+1} = & f(c_{1,ijk}^{n+1}) + \frac{1}{4}c_{1,ijk}^{n+1} - \frac{1}{4}c_{1,ijk}^n - \epsilon^2 \Delta_h c_{1,ijk}^{n+1} \\ & - c_{1,ijk}^n (1 - c_{1,ijk}^n - c_{3,ijk}^n) c_{3,ijk}^n, \end{aligned} \tag{11}$$

where the discrete Laplacian is given as $\Delta_h \phi_{ijk} = (\phi_{i+1,j,k} + \phi_{i-1,j,k} + \phi_{i,j+1,k} + \phi_{i,j-1,k} + \phi_{i,j,k+1} + \phi_{i,j,k-1} - 6\phi_{ijk})/h^2$ for $i = 1, \dots, N_x, j = 1, \dots, N_y$, and $k = 1, \dots, N_z$. At the boundary, we implement the zero Neumann boundary condition (5) as follows:

$$\begin{aligned} c_{1,0jk} &= c_{1,1jk}, & c_{1,N_x+1,jk} &= c_{1,N_xjk}, & c_{1,i0k} &= c_{1,i1k}, \\ c_{1,i,N_y+1,k} &= c_{1,iN_yk}, & c_{1,ij0} &= c_{1,ij1}, & c_{1,ij,N_z+1} &= c_{1,ijN_z}, \\ \mu_{1,0jk} &= \mu_{1,1jk}, & \mu_{1,N_x+1,jk} &= \mu_{1,N_xjk}, & \mu_{1,i0k} &= \mu_{1,i1k}, \\ \mu_{1,i,N_y+1,k} &= \mu_{1,iN_yk}, & \mu_{1,ij0} &= \mu_{1,ij1}, & \mu_{1,ij,N_z+1} &= \mu_{1,ijN_z}. \end{aligned}$$

4. Numerical experiments

In this section, we investigate the numerical solution in the two- and three-dimensional complex domains. Unless otherwise specified, we use the value of ϵ as $\epsilon_m = hm/[4\sqrt{2} \tanh^{-1}(0.9)]$ to define that the number of grid points across the interfacial regions is approximately m [40].

4.1. Effect of mesh size

First, we investigate the effect of mesh size on an artificial layer on a disk domain. We use four mesh grids: $h = 1/32$, $h = 1/64$, $h = 1/128$, and $h = 1/256$ on the whole domain $\Omega = (-0.5, 0.5) \times (-0.5, 0.5)$. Other parameters are $\Delta t = 1.5259e - 5$ and $\epsilon = \epsilon_4$. The computation is performed until the numerical solution is in the numerical equilibrium state. We defined the numerical equilibrium state if

$$\|c_1^{n+1} - c_1^n\|_2 = \sqrt{h^2 \sum_{i=1}^{N_x} \sum_{j=1}^{N_y} (c_{1,ij}^{n+1} - c_{1,ij}^n)^2} < tol,$$

where tol is a given tolerance. Here, we use $tol = 1e - 5$. The initial conditions are taken as

$$c_3(x, y) = 0.5 + 0.5 \tanh\left(\frac{\sqrt{x^2 + y^2} - 0.4}{2\sqrt{2}\epsilon}\right),$$

$$c_1(x, y, 0) = \begin{cases} 1 - c_3(x, y) & \text{if } y < 0, \\ 0 & \text{otherwise,} \end{cases}$$

$$c_2(x, y, 0) = 1 - c_1(x, y, 0) - c_3(x, y).$$

Fig. 2(a)–(d) show the numerical equilibrium state results for $h = 1/32$, $h = 1/64$, $h = 1/128$, and $h = 1/256$, respectively. Fig. 2(e)–(h) are the corresponding enlarged views of the box regions in (a), (b), (c), and (d), respectively. As we can see, an artificial layer is getting smaller as we refine the grid. Here, we alternatively solve the governing equations (see Section 4.7).

4.2. Two-dimensional disk domain

In this test, we consider the phase separation in the following disk domain, $\tilde{\Omega} = \{(x, y) | \sqrt{x^2 + y^2} < 0.45\}$. To do this, we set the computational domain as the unit square $\Omega = (-0.5, 0.5) \times (-0.5, 0.5)$, which embeds the disk domain $\tilde{\Omega}$, with zero

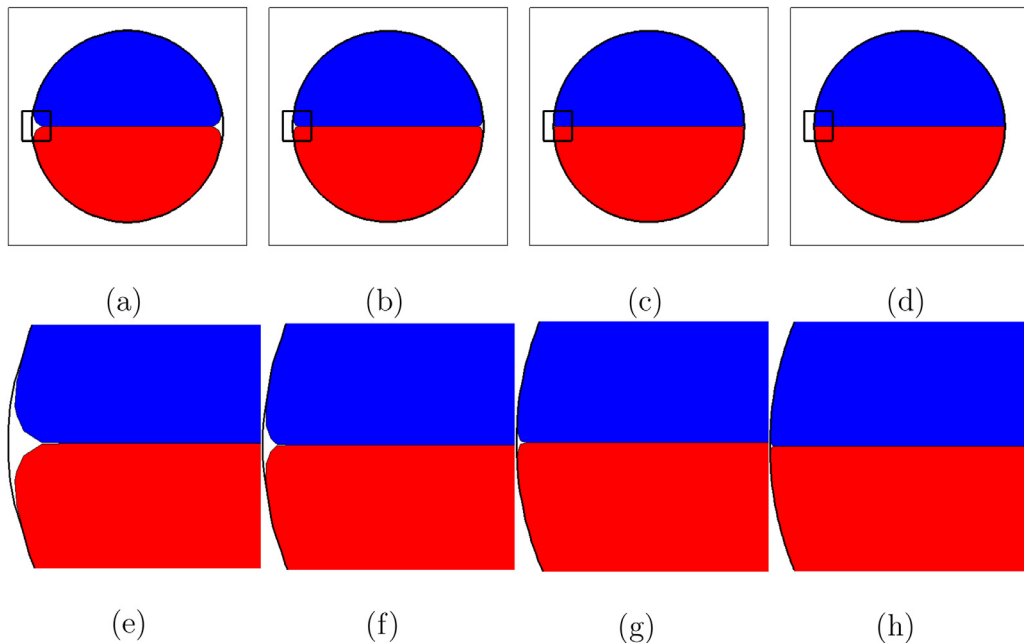


Fig. 2. Phase evolutions at numerical equilibrium state for various mesh size.

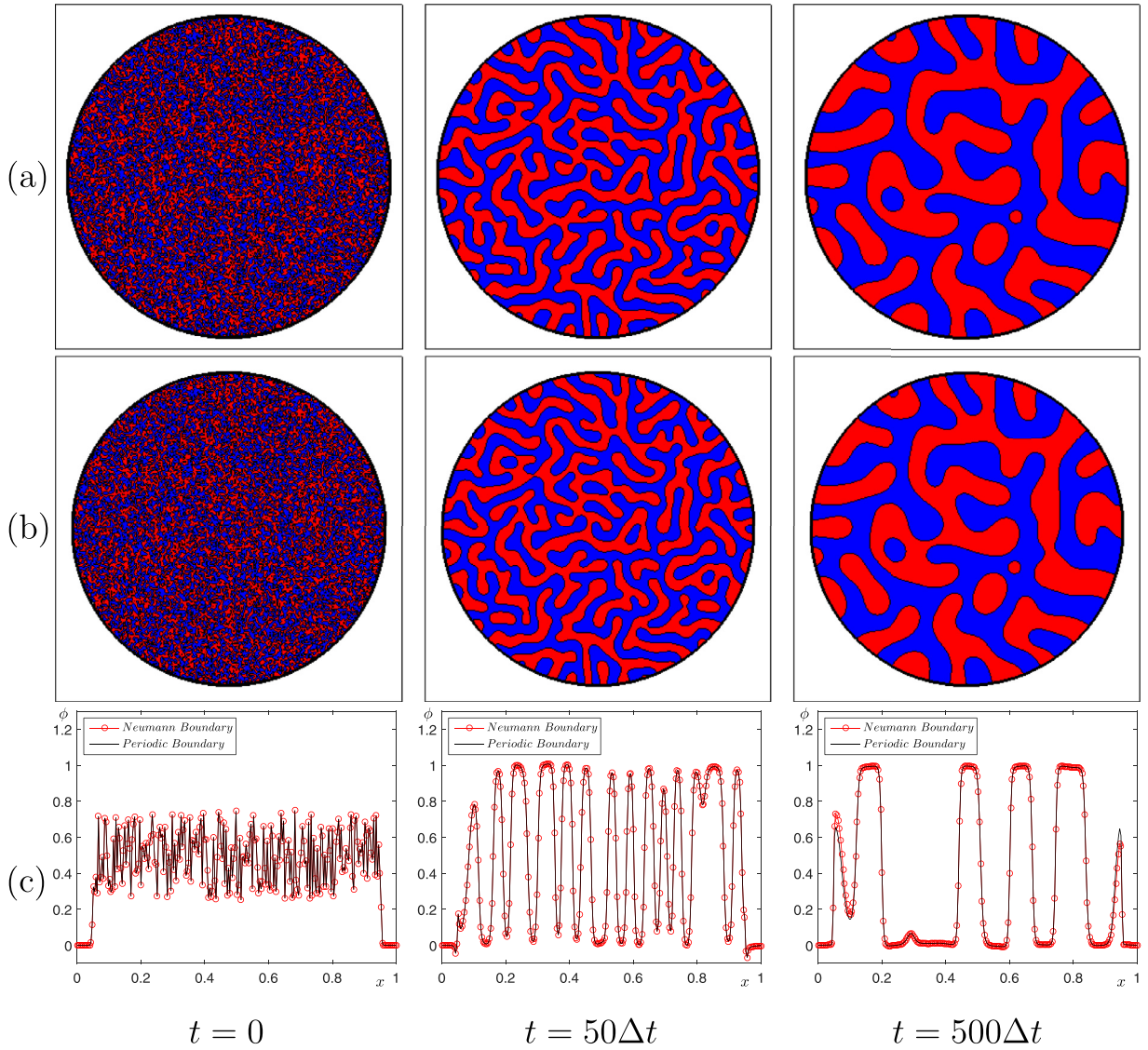


Fig. 3. Temporal evolutions of c_1 (the red region) and c_2 (the blue region) in a disk domain with (a) zero Neumann and (b) periodic boundary conditions. (c) corresponding cross sections at $y = 0$. For interpretation of the references to color in this figure, the reader is referred to the web version of this article. (For interpretation of the references to colour in this figure legend, the reader is referred to the web version of this article.)

Neumann boundary condition. Now, the initial conditions for each component are taken to be

$$c_3(x, y) = 0.5 + 0.5 \tanh \left(\frac{\sqrt{x^2 + y^2} - 0.45}{2\sqrt{2}\epsilon} \right),$$

$$c_1(x, y, 0) = [1 - c_3(x, y)][0.5 + 0.5\text{rand}(x, y)],$$

$$c_2(x, y, 0) = 1 - c_1(x, y, 0) - c_3(x, y),$$

where $\text{rand}(x, y)$ denotes a random number between -1 and 1 . Note that the disk domain is expressed by $\tilde{\Omega} = \{(x, y) | c_3(x, y) < 0.5\}$. For this numerical test, we use $h = 1/256$, $\Delta t = 10h^2$, and $\epsilon = \epsilon_4$. First, we investigate the effect of the boundary condition at $\partial\Omega$. For comparison, we implement additional test with periodic boundary condition at $\partial\Omega$ under the same parameters of the above test. Numerical results with the zero Neumann and the periodic boundary conditions are shown in the first and second rows in Fig. 3, respectively. Both of numerical temporal phase separations are almost identical as shown in Fig. 3(a) and (b) at time $t = 0, 50\Delta t$, and $500\Delta t$. We can ensure these facts in Fig. 3(c), that is, the corresponding cross sections at $y = 0$ of the numerical solutions with zero Neumann and periodic boundary conditions are

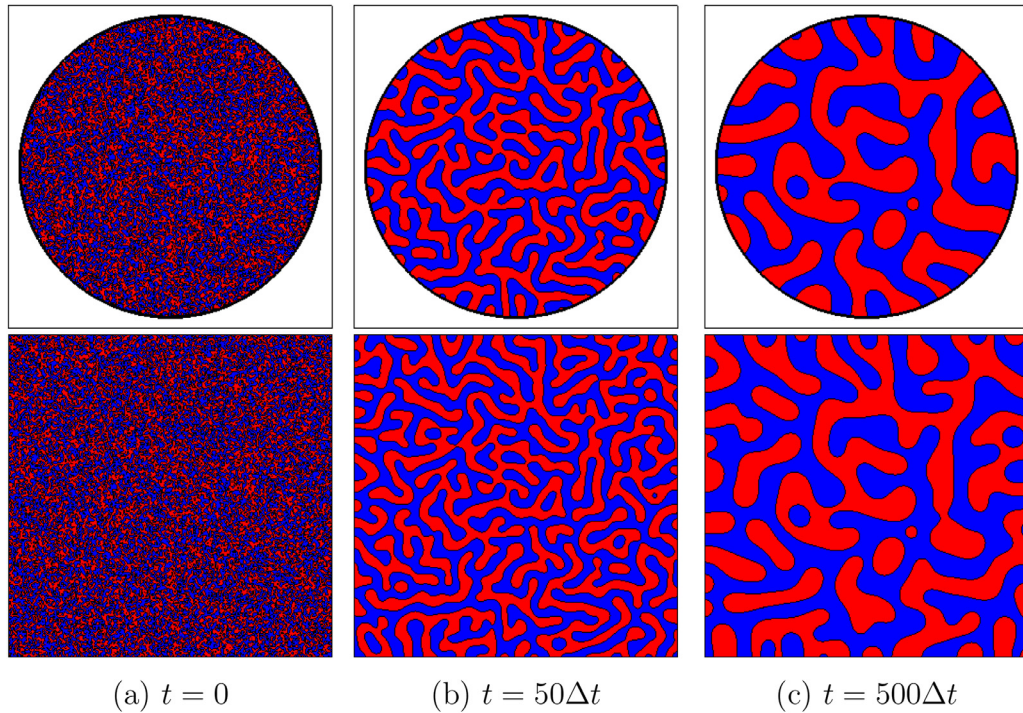


Fig. 4. Phase separations in a disk domain (the first row) and a rectangle domain (the second row) at time $t = 0, 50\Delta t$, and $500\Delta t$.

in good agreement with each other. We can see that the boundary conditions do not affect the phase separation in the disk domain. Therefore, in this study, we will use the zero Neumann boundary condition.

Furthermore, in order to confirm the general dynamics of CH equation in a complex domain, we compare the temporal evolutions of CH equation with Neumann boundary condition in a disk domain and a rectangle domain. In the case of rectangle domain, we set $c_3(x, y) = 0$, the initial conditions for $c_1(x, y, 0)$ and $c_2(x, y, 0)$ are the same as above, and the other parameters are unchanged. The first and second rows in Fig. 4 show the temporal evolutions of c_1 and c_2 in the disk and the rectangle domains, respectively. We can find the phase separations are almost same, therefore, the general dynamics of CH equation in a complex domain is conserved.

4.3. Two-dimensional brain section domain

Next, we explore the phase separation in a more complex two-dimensional domain. As an example, we consider the following brain section image [41] (see Fig. 5(a)) as a complex domain $\tilde{\Omega}$. The computational domain is defined by $\Omega = (-0.5, 0.5) \times (-0.5, 0.5)$. The parameters are chosen as follows: $h = 1/256$, $\Delta t = 10h^2$, and $\epsilon = \epsilon_4$. To define c_3 , we first segment the gray scale brain section image by a threshold into zero or one. Then, we smooth the step function by using the CH equation without the source term. That is, we evolve the CH equation with the initial profile of c_3 for 10 time step iterations and then take the final result as $c_3(x, y)$ (see Fig. 5(b) for $\tilde{\Omega} = \{(x, y) | c_3(x, y) < 0.5\}$). The gray colored region in Fig. 5(b) represents the complex domain $\tilde{\Omega}$. Therefore, in this problem, the initial conditions are

$$\begin{aligned} c_1(x, y, 0) &= [1 - c_3(x, y)][0.5 + 0.5\text{rand}(x, y)], \\ c_2(x, y, 0) &= 1 - c_1(x, y, 0) - c_3(x, y). \end{aligned}$$

As shown in Fig. 5(c)–(e), we can see the temporal evolutions of the phase c_1 in the complex brain domain $\tilde{\Omega}$ at time $t = 0, 50\Delta t$, and $500\Delta t$, respectively. Although the given brain domain is complicated, the phase separations are well done. In particular, because this method does not need to explicitly treat the boundary condition at boundary of brain domain, it is very efficient and simple to solve the CH equation.

4.4. Three-dimensional spherical domain

Now, we consider numerical tests in the three-dimensional domain. We examine the phase separation in a simple three-dimensional spherical domain $\tilde{\Omega} = \{(x, y, z) | \sqrt{x^2 + y^2 + z^2} < 0.45\}$. The whole computational domain is given as

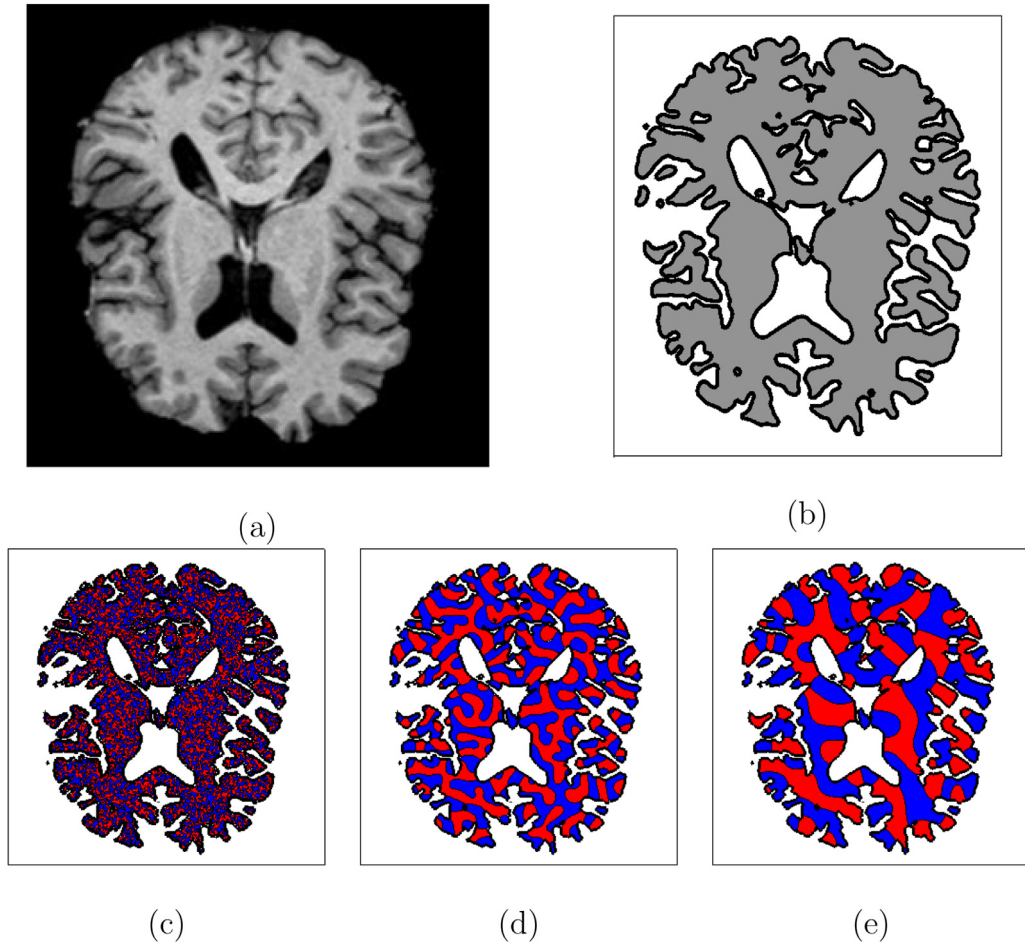


Fig. 5. Phase separation in the two-dimensional complex domain: (a) Brain section image obtained from [41] with permission from Hindawi Publishing Corporation, (b) computational domain, and (c)–(e) temporal evolutions of c_1 (the red region) and c_2 (the blue region) at $t = 0, 50\Delta t, 500\Delta t$, respectively. For interpretation of the references to colour in this figure legend, the reader is referred to the web version of this article.

$\Omega = (-0.5, 0.5) \times (-0.5, 0.5) \times (-0.5, 0.5)$. The initial condition is taken to be:

$$c_3(x, y, z) = 0.5 + 0.5 \tanh \left(\frac{\sqrt{x^2 + y^2 + z^2} - 0.45}{2\sqrt{2}\epsilon} \right),$$

$$c_1(x, y, z, 0) = [1 - c_3(x, y, z)][0.5 + 0.5\text{rand}(x, y, z)],$$

$$c_2(x, y, z, 0) = 1 - c_1(x, y, z, 0) - c_3(x, y, z),$$

where $\text{rand}(x, y, z)$ denotes a random number between -1 and 1 . In this test, we use $h = 1/128$, $\Delta t = 10h^2$, and $\epsilon = \epsilon_4$. Fig. 6(a)–(c) represent the phase separation in the spherical domain at $t = 0, 25\Delta t$, and $500\Delta t$, respectively.

4.5. Three-dimensional torus domain

We consider the phase separation in a three-dimensional torus region $\tilde{\Omega} = \{(x, y, z) | \sqrt{(\sqrt{x^2 + y^2} - 0.3)^2 + z^2} < 0.15\}$ in the computational domain $\Omega = (-0.5, 0.5) \times (-0.5, 0.5) \times (-0.25, 0.25)$. Here, we use $256 \times 256 \times 128$ mesh grid, $h = 1/256$, $\Delta t = 10h^2$, and $\epsilon = \epsilon_4$. The initial conditions are set to

$$c_3(x, y, z) = 0.5 + 0.5 \tanh \left(\frac{\sqrt{(\sqrt{x^2 + y^2} - 0.3)^2 + z^2} - 0.15}{2\sqrt{2}\epsilon} \right),$$

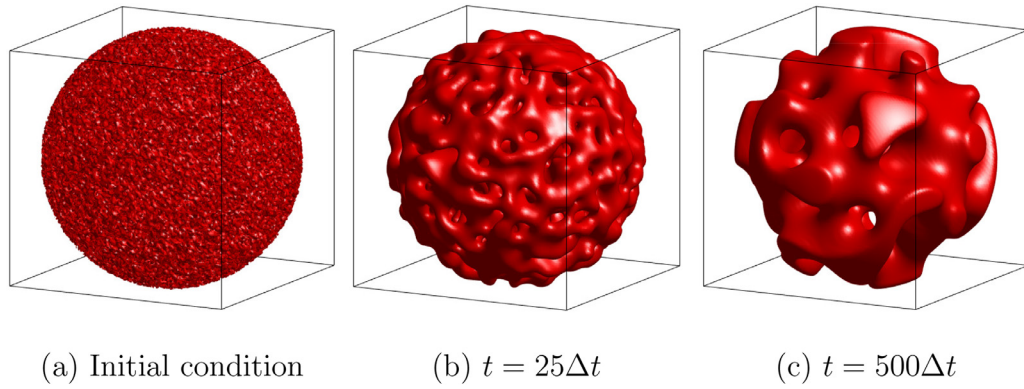


Fig. 6. Phase separation in a spherical domain.

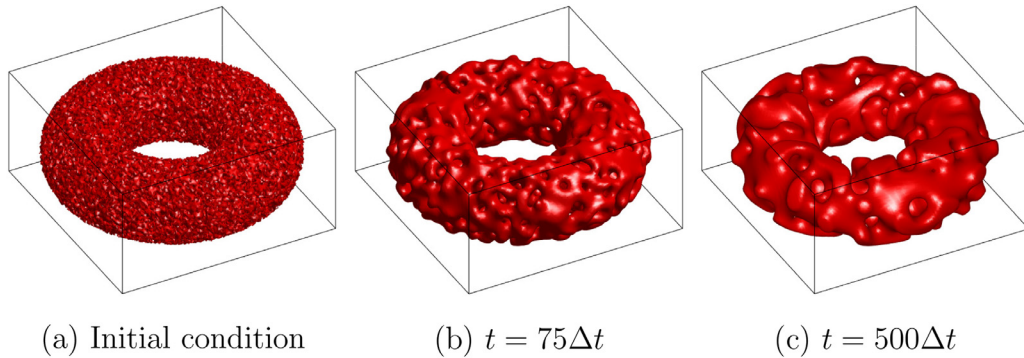


Fig. 7. Phase separation in a torus domain.

$$c_1(x, y, z, 0) = [1 - c_3(x, y, z)][0.5 + 0.5\text{rand}(x, y, z)],$$

$$c_2(x, y, z, 0) = 1 - c_1(x, y, z, 0) - c_3(x, y, z).$$

Fig. 7(a)–(c) show the phase separation in the torus domain at $t = 0, 75\Delta t,$ and $500\Delta t,$ respectively.

4.6. Three-dimensional Schwarz P, Schwarz D, and Schoen G domains

Next, we consider some more complex three-dimensional domains such as Schwarz P, Schwarz D, and Schoen G domains [42]. In the computational domain $\Omega = (0, 1) \times (0, 1) \times (0, 1),$ the parameters used are the same with the above three-dimensional tests. We define the initial conditions as

$$c_3(x, y, z) = 0.5 + 0.5 \tanh\left(\frac{\phi(x, y, z)}{20\sqrt{2}\epsilon}\right),$$

$$c_1(x, y, z, 0) = [1 - c_3(x, y, z)][0.5 + 0.5\text{rand}(x, y, z)],$$

$$c_2(x, y, z, 0) = 1 - c_1(x, y, z, 0) - c_3(x, y, z),$$

where

$$\phi(x, y, z) = \cos 2\pi x + \cos 2\pi y + \cos 2\pi z,$$

$$\phi(x, y, z) = \cos 2\pi x \cos 2\pi y \cos 2\pi z - \sin 2\pi x \sin 2\pi y \sin 2\pi z, \quad \text{and}$$

$$\phi(x, y, z) = \sin 2\pi x \cos 2\pi y + \sin 2\pi z \cos 2\pi x + \sin 2\pi y \cos 2\pi z$$

are for Schwarz P, Schwarz D, and Schoen G domains, respectively. Fig. 8 shows phase separation in (a) the Schwarz P, (b) the Schwarz D, and (c) the Schoen G domains. Here, the first, second, and third rows are snapshots of the numerical results at $t = 0, 10\Delta t, 290\Delta t,$ respectively, on the given complex domain $\tilde{\Omega}.$

4.7. Three-dimensional Menger sponge domain

As the final example, we consider a three-dimensional complex domain, the Menger sponge domain [43] (see Fig. 9).

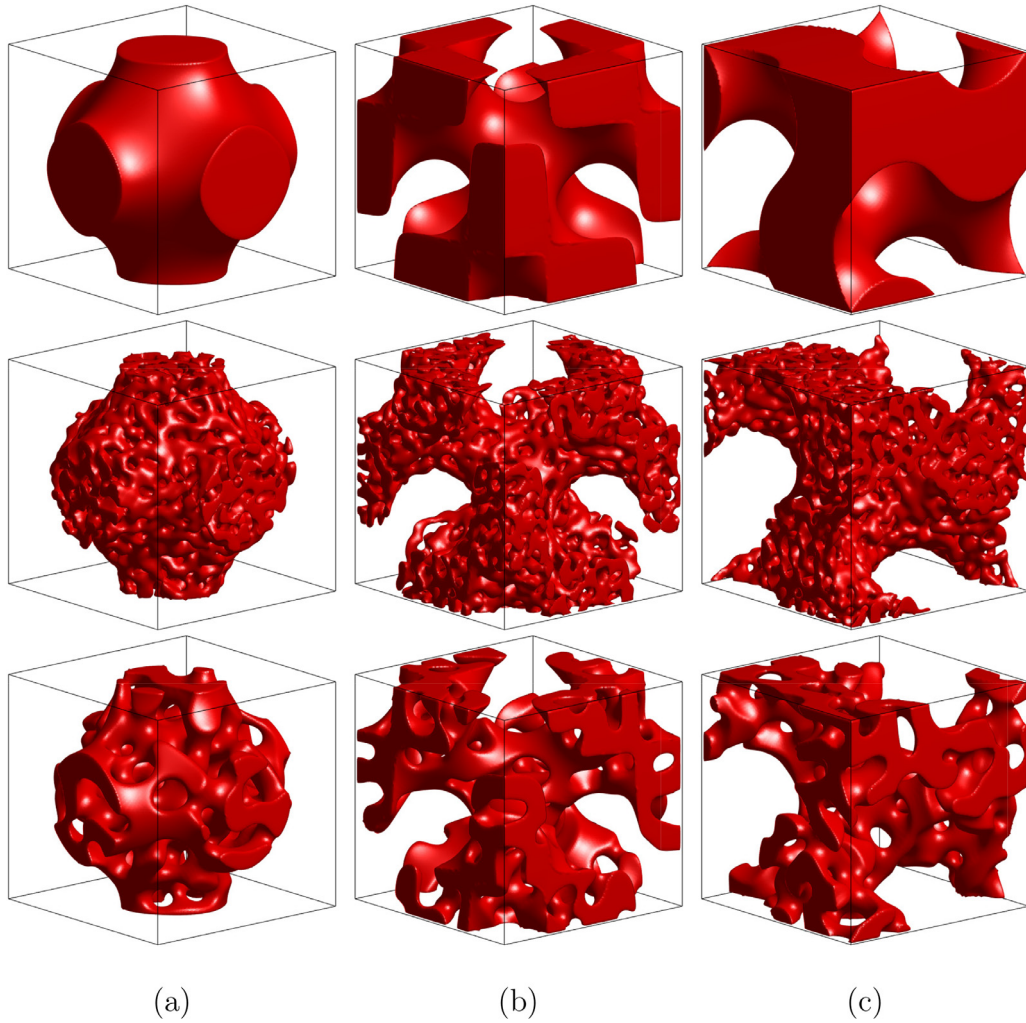


Fig. 8. Phase separation in (a) Schwarz P, (b) Schwarz D, and (c) Schoen G domains. Here, the first, second, and third rows are snapshots of numerical result on each complex domain $\tilde{\Omega}$ at $t = 0, 10\Delta t, 290\Delta t$, respectively.

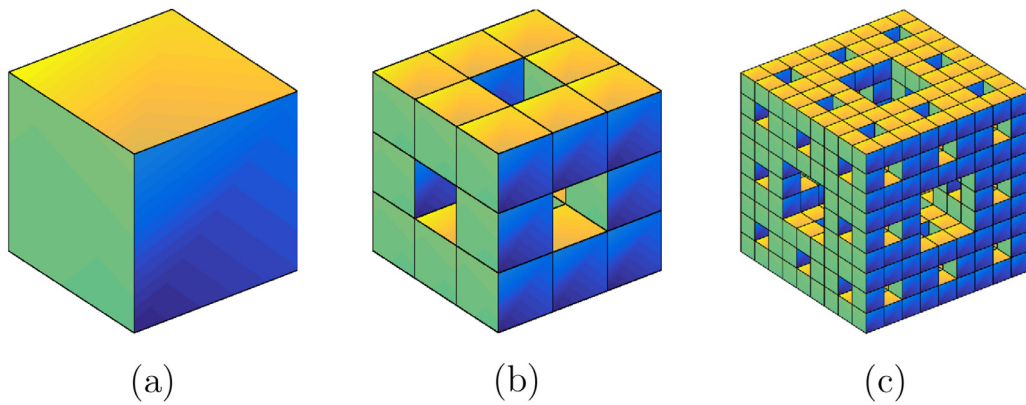


Fig. 9. Menger cube with level (a) 0, (b) 1, and (c) 2.

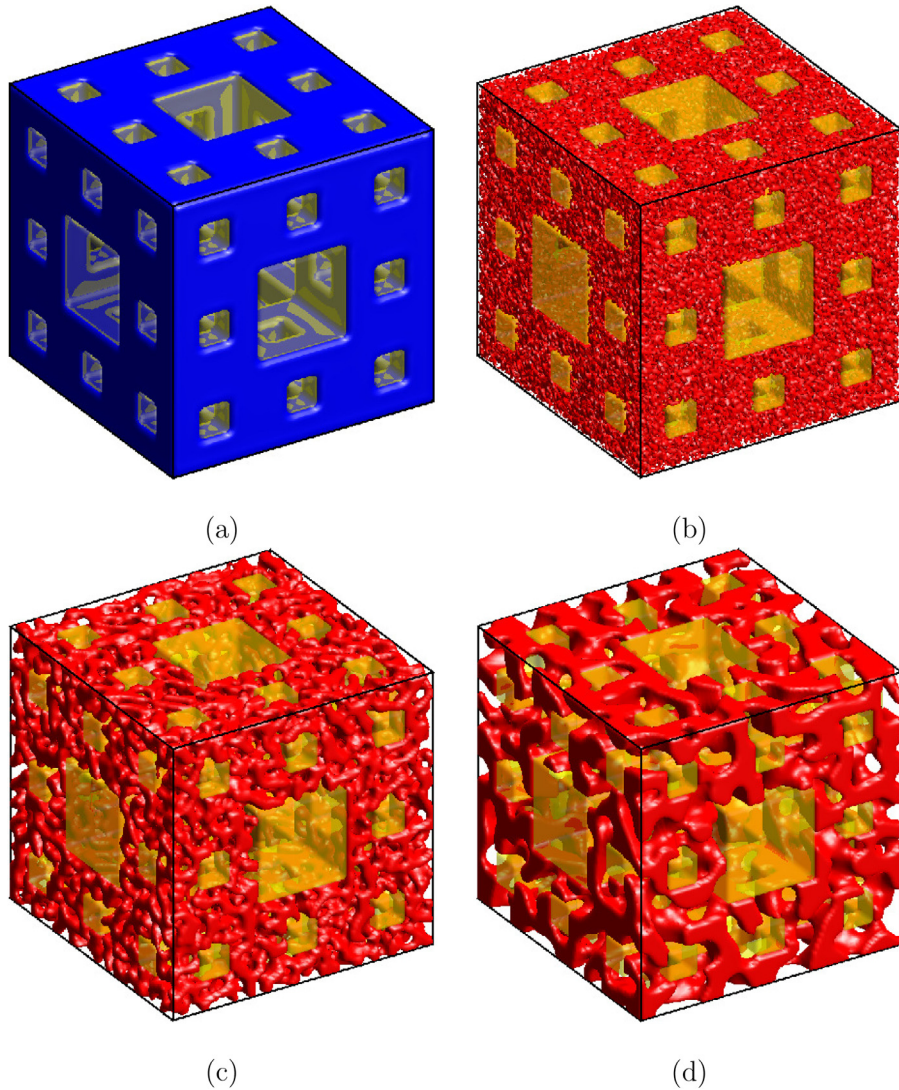


Fig. 10. Phase separation in the Menger cube domain. (a) Level-2 Menger sponge, (b)–(d): Isosurface of numerical solution c_1 at 0.5-level at time $t = 0$, $50\Delta t$, and $500\Delta t$, respectively.

We use the Menger sponge domain with level 2 as shown in Fig. 9(c) and the length of one side of the Menger sponge domain is $234/256$. We embed this Menger sponge domain in the computational domain $\Omega = (0, 1) \times (0, 1) \times (0, 1)$. We use the following parameters: $h = 1/256$, $\Delta t = 10h^2$, and $\epsilon = \epsilon_4$. The initial conditions are

$$c_3(x, y, z) = \begin{cases} 0 & \text{inside the Menger sponge domain,} \\ 1 & \text{otherwise,} \end{cases}$$

$$c_1(x, y, z, 0) = [1 - c_3(x, y, z)][0.5 + 0.5\text{rand}(x, y, z)],$$

$$c_2(x, y, z, 0) = 1 - c_1(x, y, z, 0) - c_3(x, y, z).$$

If the initial condition of c_3 is not smooth and is given by a step function, the numerical solution c_1 has a bias result nearby the boundary of the domain $\hat{\Omega}$. Therefore, to remove this bias problem, we alternatively solve Eqs. (10) and (11) for c_1 and c_2 . That is, we solve the equations for c_1 ; and then set $c_2 = 1 - c_1 - c_3$ and solve the equations for c_2 . Next, we set $c_1 = 1 - c_2 - c_3$ and solve the equations for c_1 . By alternatively solving the equations for c_1 and c_2 , we successively remove the bias problem. As shown in Fig. 10, the proposed numerical algorithm performs well in the complex domain with sharp curvatures.

Until now, we implement the several numerical test on various complex domains. Through these test, we can see that our method is very simple and efficient to solve the CH equation in a complex domain because we do not explicitly treat the boundary conditions at the complex domain.

5. Conclusions

In this study, we proposed an efficient numerical method for the CH equation in the two- and three-dimensional arbitrary domains. The proposed mathematical model is based on the ternary CH system. The main idea is that we represent arbitrary domains with the third phase in the ternary system and solve the binary CH equation with a source term. The numerical results demonstrated that the proposed algorithm can deal with the complex domains efficiently. Furthermore, after a small modification of the pre-existing codes such as Fourier spectral method, finite element method, and isogeometric method for the CH equation, the proposed algorithm can be straightforwardly implemented. The methodology proposed in this paper can be used in generating three-dimensional bio-scaffolds and multiphase fluid flows with arbitrary structures. As future work, we will improve the proposed method by controlling the contact angle in the complex domain with the free energy functional.

Acknowledgments

The authors thank the reviewers for their constructive and helpful comments on the revision of this article. The first author (D. Jeong) was supported by the [National Research Foundation of Korea \(NRF\)](#) grant funded by the Korea government (MSIP) (NRF-2017R1E1A1A03070953). The corresponding author (Junseok Kim) was supported by [Basic Science Research Program](#) through the [National Research Foundation of Korea \(NRF\)](#) funded by the [Ministry of Education](#) (NRF-2016R1D1A1B03933243).

References

- [1] Li Y, Kim J. Multiphase image segmentation using a phase-field model. *Comput Math Appl* 2011;62(2):737–45.
- [2] Cahn JW. On spinodal decomposition. *Acta Metall* 1961;9:795–801.
- [3] Allen SM, Cahn JW. A microscopic theory for antiphase boundary motion and its application to antiphase domain coarsening. *Acta Metall* 1979;27:1085–95.
- [4] Kou J, Sun S. Thermodynamically consistent modeling and simulation of multi-component two-phase flow with partial miscibility. *Comput Meth Appl Mech Eng* 2018;331:623–49.
- [5] Kim J, Lee S, Choi Y, Lee SM, Jeong D. Basic principles and practical applications of the Cahn–Hilliard equation. *Math Probl Eng* 2016;1–11. Article ID 9532608
- [6] Li Y, Kim J, Wang N. An unconditionally energy-stable second-order time-accurate scheme for the Cahn–Hilliard equation on surfaces. *Commun Nonlinear Sci Numer Simul* 2017;53:213–27.
- [7] Dehghan M, Mohammadi V. Comparison between two meshless methods based on collocation technique for the numerical solution of four-species tumor growth model. *Commun Nonlinear Sci Numer Simul* 2017;44:204–19.
- [8] Haji AH, Mahzoon M, Javadpour S. Pattern formation and geometry of the manifold. *Commun Nonlinear Sci Numer Simul* 2011;16:1424–32.
- [9] Jaensson NO, Hulsen MA, Anderson PD. Stokes–Cahn–Hilliard formulations and simulations of two-phase flows with suspended rigid particles. *Comput Fluids* 2015;111:1–17.
- [10] Bai F, He X, Yang X, Zhou R, Wang C. Three dimensional phase-field investigation of droplet formation in microfluidic flow focusing devices with experimental validation. *Int J Multiphase Flow* 2017;93:130–41.
- [11] Lee D, Huh JY, Jeong D, Shin J, Yun A, Kim J. Physical, mathematical, and numerical derivations of the Cahn–Hilliard equation. *Comput Mater Sci* 2014;81:216–25.
- [12] Jeong D, Choi Y, Kim J. A benchmark problem for the two-and three-dimensional Cahn–Hilliard equations. *Commun Nonlinear Sci Numer Simul* 2018;61:149–59.
- [13] Areias P, Samaniego E, Rabczuk T. A staggered approach for the coupling of Cahn–Hilliard type diffusion and finite strain elasticity. *Comput Mech* 2016;57:339–51.
- [14] Chan C, Anitescu C, Rabczuk T. Isogeometric analysis with strong multipatch c^1 -coupling. *Comput Aided Geom D* 2018;62:294–310.
- [15] Shin J, Jeong D, Kim J. A conservative numerical method for the Cahn–Hilliard equation in complex domains. *J Comput Phys* 2011;230:7441–55.
- [16] Li Y, Jeong D, Shin J, Kim J. A conservative numerical method for the Cahn–Hilliard equation with dirichlet boundary conditions in complex domains. *Comput Math Appl* 2013;65:102–15.
- [17] Aland S, Lowengrub J, Voigt A. Two-phase flow in complex geometries: a diffuse domain approach. *Comput Model Eng Sci* 2010;57:77–106.
- [18] Li D, Qiao Z. On second order semi-implicit fourier spectral methods for 2d Cahn–Hilliard equations. *J Sci Comput* 2017;70:301–41.
- [19] Li D, Qiao Z, Tang T. Characterizing the stabilization size for semi-implicit fourier-spectral method to phase field equations. *SIAM J Numer Anal* 2016;54:1653–81.
- [20] Li D, Qiao Z. On the stabilization size of semi-implicit fourier-spectral methods for 3d Cahn–Hilliard equations. *Commun Math Sci* 2017;15:1489–506.
- [21] Diegel A, Wang C, Wise SM. Stability and convergence of a second-order mixed finite element method for the Cahn–Hilliard equation. *IMA J Numer Anal* 2016;36:1867–97.
- [22] Diegel A, Feng X, Wise SM. Analysis of a mixed finite element method for a Cahn–Hilliard–Darcy–Stokes system. *SIAM J Numer Anal* 2015;53:127–52.
- [23] Diegel A, Wang C, Wang X, Wise SM. Convergence analysis and error estimates for a second order accurate finite element method for the Cahn–Hilliard–Navier–Stokes system. *Numer Math* 2017;137:495–534.
- [24] Sariaydin-Filibelioglu A, Karasözen B, Uzunca M. Energy stable interior penalty discontinuous Galerkin finite element method for Cahn–Hilliard equation. *Commun Nonlinear Sci Numer Simul* 2017;18:303–14.
- [25] Kästner M, Metsch P, de Borst R. Isogeometric analysis of the Cahn–Hilliard equation—a convergence study. *J Comput Phys* 2016;305:360–71.
- [26] Bartezzaghi A, Dedé L, Quarteroni A. Isogeometric analysis of high order partial differential equations on surfaces. *Comput Methods Appl Mech Eng* 2015;295:446–69.
- [27] Zhao Y, Schillinger D, Xu BX. Variational boundary conditions based on the Nitsche method for fitted and unfitted isogeometric discretizations of the mechanically coupled Cahn–Hilliard equation. *J Comput Phys* 2017;340:177–99.
- [28] Elliott CM, Garcke H. Diffusional phase transitions in multicomponent systems with a concentration dependent mobility matrix. *Phys D* 1997;109(3–4):242–56.
- [29] Garcke H, Nestler B, Stoth B. On anisotropic order parameter models for multiphase systems and their sharp interface limits. *Phys D* 1998;115:87–108.
- [30] Lee HG, Kim J. A second-order accurate non-linear difference scheme for the n-component Cahn–Hilliard system. *Phys A* 2008;387:19–20.
- [31] Chockalingam K, Kouznetsova VG, van der SO, Geers MGD. 2D phase field modeling of sintering of silver nanoparticles. *Comput Methods Appl Mech Eng* 2016;312:492–508.
- [32] Vignal P, Collier N, Dalcin L, Brown DL, Calo VM. An energy-stable time-integrator for phase-field models. *Comput Methods Appl Mech Eng* 2017;316:1179–214.

- [33] Guo Z, Lin P, Lowengrub J, Wise SM. Mass conservative and energy stable finite difference methods for the quasi-incompressible navier–stokes–Cahn–Hilliard system: primitive variable and projection type schemes. *Comput Methods Appl Mech Eng* 2017;326:144–74.
- [34] Baskaran A, Guan Z, Lowengrub J. Energy stable multigrid method for local and non-local hydrodynamic models for freezing. *Comput Methods Appl Mech Eng* 2016;299:22–56.
- [35] Hirschler M, Huber M, Säckel W, Kunz P, Nieken U. An application of the Cahn–Hilliard approach to smoothed particle hydrodynamics. *Math Probl Eng* 2014:1–10. Article ID 694894
- [36] Eyre DJ. Unconditionally gradient stable time marching the Cahn–Hilliard equation. In: Bullard JW, Chen LQ, editors. *Computational and mathematical models of microstructural evolution*, in: MRS proceedings, vol. 529. Cambridge University Press; 1998. p. 39–46.
- [37] Lee HG, Choi JW, Kim J. A practically unconditionally gradient stable scheme for the n-component Cahn–Hilliard system. *Phys A* 2012;391:1009–19.
- [38] Trottenberg U, Oosterlee C, Schüller A. *Multigrid*. London: Academic Press; 2001.
- [39] Kim J. A numerical method for the Cahn–Hilliard equation with a variable mobility. *Commun Nonlinear Sci Numer Simul* 2007;12:1560–71.
- [40] Kim J. Phase-field models for multi-component fluid flows. *Commun Comput Phys* 2012;12:613–61.
- [41] Despotović I, Goossens B, Philips W. MRI segmentation of the human brain: challenges, methods, and applications. *Comput Math Methods Med* 2015:1–23. Article ID 450341
- [42] Gandy PJ, Bardhan S, Mackay AL, Klinowski J. Nodal surface approximations to the p, g, d and i-WP triply periodic minimal surfaces. *Chem Phys Lett* 2001;336:187–95.
- [43] Feder J. *Fractals*. New York: Plenum Press; 1988.